IUST
Iran University of
Science and Technology

A Dynamic Control Approach for AC Micro-Grids Including Non-Inverter and Inverter Based Energy Resources

Z. Mobini-Serajy*, M. Radmehr**(C.A.), and A. Ghorbani**

Abstract: Micro-Grids harness the benefits of non-inverter and inverter based Distributed Energy Resources (DER) in grid-connected and island environments. Adoption them with the various type of electric loads in modern MGs has led to stability and power quality issues. In this paper, two-level control approach is proposed to overcome these problems. A state-space dynamic model is performed for Micro-Grids, for this goal, the state-space equations for generation, network and load components are separately developed in a local DQ reference frame, and after linearization around the set point, then combining them into a common DQ reference frame. In the first level, the control of inverter-based DERs and some types of loads with fast response are activated, and in the second level, the control of synchronous diesel generator resources with slower response are used. In order to validate and effectiveness evaluation of proposed control approach, numerical studies have been stablished on a standard test MG under normal and a symmetrical three-phase fault conditions. Finally, the simulations results are summarized.

1. Introduction

Today, the demand for electrical energy with high reliability and proper quality is felt more than previous years. Due to the depletion of fossil resources, environmental pollution, depreciation of the existing equipment of transmission, sub-transmission and distribution networks, and the need to invest for the expansion of the power network as well as grantee the costumers reliability, therefore, many countries in the world move toward renewable energy resources including wind turbines, solar power plants, micro turbines, energy storage devices such as batteries, which are the most important resources of electrical energy.

The penetration of these resources in the distribution network has led to the creation of active distribution networks. With the use of advanced telecommunication and control devices, active distribution networks were able to provide their local load demands and convert to Micro Grid (MG) that can operate grid-connected and islanded modes [1]. Sometimes, in a MG, Distributed Energy Resources (DERs) provide significant amount of active and reactive load demand, therefore, their dynamic behaviors have strong effect on system voltage and frequency during contingency events. Considering the different dynamics of small DERs compare to large power plants, their impact on the dynamics of the MG will be different. Often, MGs face with the number of stability issues including frequency stability, voltage stability, and transient stability which are crucial for ensuring the safe and reliable operation. Considering stability issues, we can improve the performance of MG, enhance their ability to integrate renewable energy resources, and ensure their long-term viability as a sustainable energy solution. With the high penetration of non-inverter and inverter based DERs in form of MGs, the power system inertia is compromised and causing

stability issues. Several approaches for system inertia are introduced such as virtual inertia support to suppress the fast changes in frequency and DC voltages to enhance the MG stability. In reference [2], a hierarchical stochastic frequency constrained micro-market model has proposed for isolated MGs. In reference [3], a precise and very fine-tune hierarchical controls used to manage the active and reactive power along with scheduling of primary and secondary reserves to ensure MG stability. Inverter based DERs can be correctly regulated to compensate for harmonics and voltage imbalance in the MGs. It is assumed that this instability may occur due to system overload with bulk dynamic load, power quality issues, unbalanced compensation for critical buses and etc. The stability issues are divided two categories based on the primary layer (consumer) and the secondary layer (generation). The primary layer deals with the power quality, reliability, and consumer end price. The secondary layer represents voltage stability, synchronization in frequency, and protection system. Get to secondary layer stability in MGs can ensure the stability of the primary layer, automatically. The main goal of frequency control in MGs is to synchronize the frequency of non-inverter and inverter based DERs to a common set point (nominal frequency). Frequency deviations in the MGs interfaced power networks occur due to variable power output of DERs, load variations, demand and voltage fluctuations. For frequency stability, a realistic approach for estimating the non-synchronous inertial response is proposed which allows the operator to select the best inertial response of the system for stable operation. A proportional integral and distributed proportional controllers are developed for frequency synchronization in the power network [4]. Stability situations during voltage fluctuations for droop control based on port Hamiltonian modeling are derived in [5]. Distributed frequency and voltage control is proposed in [6] for AC MG based on Primal-Dual Gradient Dynamics. Several power flow strategy is discussed in [7] for frequency synchronization and voltage control of islanded MGs. Detailed analysis of frequency deviations due to voltage fluctuations (drops, sags, collapse, and overvoltage) is discussed in [8]. For frequency and voltage stability, decentralized control strategies are chosen in [9] for Autonomous MGs. The stability of hybrid AC-DC MGs is improved in [10] using nonlinear centralized control in island performance. A fully distributed control paradigm was proposed in [11] for secondary control of islanded MG. The MG system had droop controlled DG units with predominantly inductive transmission lines and different communication topologies and also the voltage and frequency restoration for inverter-based DERs are simultaneously addressed in spite of disturbances. A new

approach for MG stability analysis is proposed in [12] when MGs is connected to or disconnected from the national grid. Also, linear and non-linear MG models in different operating conditions, optimal design of the LC filter, control parameters optimization and power distribution coefficients have been analyzed in islanded operation mode. A frequency control approach is presented in [13] for MGs, in fact, it proposes a secondary frequency controller that assumes the weighted average of the frequency deviation in the load as an input, and its output value is determined with regard to generation reserves and distance of induction loads. In [14], a linear control strategy for voltage and frequency regulation is proposed for smart distribution systems and MGs including different types of DGs. The frequency and stability characteristics of the MG are investigated in [15]. An approach is proposed to analyze the inertia coefficient based on the theory of DGs close to each other with same frequency. An approach is presented in [16] for tracking the reference voltage of MG for active loads synchronization. In addition, a MGs is modeled and designed with islanding operation and the impact of active loads on the frequency stability levels of MG is cheeked. Stochastic frequency control of grid-connected MGs was discussed in [17]. The robust stability of an ac/dc hybrid MG including synchronous diesel generator sources and inverter based DERs was investigated in [18]. Main contribution of this paper is as follow: A two-level controller is proposed with a very fast response in the first level and a slower response in the second level, respectively. Since, it is very important to provide an accurate model for performance analysis, control and stability of MGs during possible events such as sudden load changes, short circuit and DGs failures and disconnection from the upstream grid. Main goal is maintaining the MG stability during off-grid operation mode after dynamic events occurrence alongside achieving the suitable power quality, simultaneously. There are inverter and non-inverter based DERs and loads with rectifier interface, constant power consumption, constant and dynamic impedances in under study MGs. Upstream national grid can exchange active and reactive powers with MG in normal operating mode. When, a fault occurs during the MG island operation, stability and frequency control of the MG cause to a challenge due to low ramping rates and the moment of inertia of the shaft of the synchronous diesel generators. Therefore, inverter-based DERs beside some types of loads with very fast response can be used at first level of our control scheme. However, switching process of inverter-based DERs causes the harmonic injection and power quality deterioration in MG, to overcome this problem, multi-level inverter with a cascade bridge structure is replaced with ordinary inverters. After the

occurrence of dynamic events such as load change or fault occurrence, redispatch of synchronous diesel generators are used at second level of our control scheme to remove the voltage and frequency offsets in the MG. Therefore, the rest of paper is organized at the contentious: In section2, the dynamic modeling of the MG including inverter-based DERs and synchronous diesel generators, network and static and dynamic loads are performed using the state space method and common DQ reference frame technique. In section3, the proposed two-level control approach will describe by the goal of MG transient stability and power quality improvement during possible contingency events. In section4, in order to the proposed model validation, numerical studies are applied on a standard test MG under different conditions such as fault occurrence, and disconnection from the upstream network, simultaneously. In section5, the simulation results are summarized and presented.

2. Dynamic Modelling of MG System

In this section, the general process of dynamic modeling for the MG system including inverter-based DGs and synchronous diesel generator with island operation from upstream network in a common DQ synchronous reference frame is described. In the proposed modeling process, the MG system is divided into three submodules: generation, network and load. Park's transformation is used to map the ABC space to the local DQ reference frame according to Eq. (1).

$$
\left[T_{dq} \right] = \sqrt{\frac{2}{3}} \begin{bmatrix} \cos(\omega t + \theta) & \cos\left(\omega t + \theta - \frac{2\pi}{3}\right) & \cos\left(\omega t + \theta + \frac{2\pi}{3}\right) \\ -\sin(\omega t + \theta) & -\sin\left(\omega t + \theta - \frac{2\pi}{3}\right) & -\sin\left(\omega t + \theta + \frac{2\pi}{3}\right) \\ \frac{1}{\sqrt{2}} & \frac{1}{\sqrt{2}} & \frac{1}{\sqrt{2}} \end{bmatrix} \quad (1)
$$

In the generalized model for MG system with non-inverter and inverter-based DERs during island operation, Indexes $n_N, n_{IIDG}, n_{DG}, n_L, n_{PL}, n_{AL}$ and n_{IM} are respectively defined as the number of nodes or buses, inverter-based DG units and synchronous diesel generators, lines, passive loads, active load and dynamic induction motor loads.

2.1 Generation Sub-Module

The generation sub-module consists of modelling the number of inverter-based DG units in their local DQ reference frame. Since, there are many inverter-based DG units in the inverter-based MG system with islanding operation, the first reference frame of the inverter-based DG unit is assumed as a common DQ reference frame, and other inverter-based DG units are transferred to this common DQ reference using the conversion technique according to Eq. (2) [19]. Here,

$(D-Q)$ is the common reference frame axis that is rotating with the frequency (ω_{com}) while $(d-q)_i$ is the local reference frame axis for ith inverter-based DG unit that is rotating with the frequency (ω_i). In Eq. (2), the indices $x_{i,dq}$ and $x_{i,DQ}$ are the state values of the ith inverter-based DG unit in local and the common reference frame, respectively. The angular difference between the mentioned reference frames (δ_i) is defined according to Eq. (3). The model of each inverter-based DG unit includes power processing and local control as shown in Fig. 1.

$$
\begin{bmatrix} x_{i,D} \\ x_{i,Q} \end{bmatrix} = \begin{bmatrix} \cos(\delta_i) & -\sin(\delta_i) \\ \sin(\delta_i) & \cos(\delta_i) \end{bmatrix} \begin{bmatrix} x_{i,d} \\ x_{i,q} \end{bmatrix} \quad (2)
$$

$$
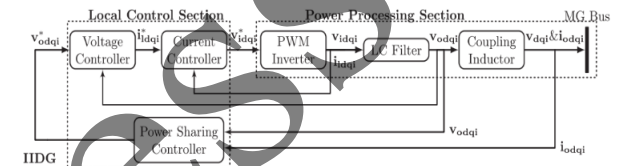\delta_i = \int(\omega_i - \omega_{com})dt, \forall i \quad (3)
$$

Fig. 1 Model for each inverter-based DG unit in MG system

The power processing part includes a three-leg voltage source inverter, LC filter and a coupling inductor, while the control part can be divided into the power distribution controller and the voltage and current controller loops. DC bus dynamics of the voltage source inverter are damped with this assumption that the DC bus voltage fluctuations by the converter on the generator side will feed from the DC voltage source inverter [20]. In addition, the switching process of the voltage source inverter is also neglected by realizing high frequency switching (4-10 kHz) [21]. The outer loop for power distribution controller is shown in Fig. 2 which can adjust the output frequency and voltage magnitude of the inverter-based DG unit, respectively, based on the characteristics of the active and reactive power drop equal with a normal synchronous generator. The reference frequency (ω_{i-dr}^*) and reference voltage $(v_{odi-dr}^*, v_{oqi-dr}^*)$ for the ith inverter-based DG unit are given in Eq. (4) and Eq. (5), respectively. The active and reactive static power droop gains of ith inverter-based DG unit for a certain range of frequency and voltage are calculated according to Eq. (6) and Eq. (7), respectively. The average value of the active P_i and reactive Q_i powers of ith inverter-based DG unit are the low-pass filter output which are computed through Eq. (8) and Eq. (9), respectively.

$$
\omega_{i-dr}^* = \omega_n - m_{Pi}P_i \quad (4)
$$

$$v^*_{odi-dr} = V_n - n_{Qi}Q_i \qquad (5)$$

$$v^*_{oqi-dr} = 0$$

$$m_{Pi} = \frac{w_{max} - w_{min}}{P_{max\,i}} \quad \forall i \qquad (6)$$

$$n_{Qi} = \frac{V_{od\,max} - V_{od\,min}}{Q_{max\,i}} \quad \forall i \qquad (7)$$

$$P_i = \frac{w_c}{s + w_c} \times 1.5\left(v_{odi}i_{odi} + v_{oqi}i_{oqi}\right) \qquad (8)$$

$$Q_i = \frac{w_c}{s + w_c} \times 1.5\left(v_{oqi}i_{odi} - v_{odi}i_{oqi}\right) \qquad (9)$$

In above relation, ω_n and V_n are the nominal setting points of the d-axis output voltage and frequency, respectively. Indexes m_{Pi} and m_{Qi} are the active and reactive static powers, respectively. To facilitate the voltage control, q-axis component of the voltage $\left(v^*_{oqi-dr}\right)$ is set to zero. In above relation, v_{odi}, v_{oqi}, i_{odi} and i_{oqi}, are the output voltages and currents of the ith inverter-based distributed generation unit in the local DQ reference frame, respectively and w_c is the cutoff frequency of the low-pass filter. The inner loop voltage and current controllers are designed to eliminate high frequency disturbances and provide sufficient damping for the LC output filter. The voltage controller produces the reference current vector of the filter inductance $\left(i^*_{ldqi}\right)$ while the current controller produces the excitation voltage vector $\left(v^*_{idqi}\right)$ in the form of a pulse width modulation module. In addition, the voltage controller is necessary to create the voltage regulation optimally, while the current controller is applied to form the voltage of the two ends of the LC filter inductor. Figure 3 shows the block diagram of the voltage and current controllers of the inner loop which includes all the forward and backward terms. Here, the voltage and current controllers use standard proportional-integral (PI) regulators to control the output voltage and output current of filter inductor, respectively. The voltage and current controllers dynamics of the inner loop ith inverter-based DG unit shown in Fig. 3 includes standard integral and proportional gains including K_{pv}, K_{iv}, K_{pi}, K_{ii} and also feedforward gain F, which are expressed as Eq. (10) to Eq. (13), respectively. Eq. (12) and Eq. (13) show the dynamic equations of the inner loop current controller. In these relations, the reference currents i^*_{ldqi} are generated using the voltage controller and are used as set point values for the inner loop of current controller. In this regard $\gamma_{dqi} = \int\left(i^*_{ldqi} - i_{ldqi}\right)dt$, the reference output voltages v^*_{ldqi} are produced by the inner loop of current controller, which are used as set point values for the pulse width modulation inverter as shown in Fig. 1.
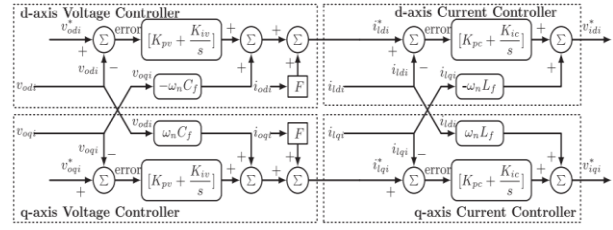

Fig. 3 Voltage and inner loop current controllers for ith inverter-based DG unit

$$i^*_{ldi} = K_{pv}\left(v^*_{odi} - v_{odi}\right) + K_{iv}\phi_{di} - v_{oqi}\omega_n C_f + Fi_{odi} \qquad (10)$$

$$i^*_{lqi} = K_{pv}\left(v^*_{oqi} - v_{oqi}\right) + K_{iv}\phi_{qi} + v_{odi}\omega_n C_f + Fi_{oqi} \qquad (11)$$

$$v^*_{idi} = K_{pi}\left(i^*_{ldi} - i_{ldi}\right) + K_{ii}\gamma_{di} - i_{lqi}\omega_n L_f \qquad (12)$$

$$v^*_{iqi} = K_{pi}\left(i^*_{lqi} - i_{lqi}\right) + K_{ii}\gamma_{qi} - i_{ldi}\omega_n L_f \qquad (13)$$

The LC low-pass filter is combined with the coupling inductance to create the output LCL filter. Coupling inductance shapes the output impedance of the PWM inverter in such a way that the coupling of active and reactive powers is minimized. The dynamics of voltage and current for the output LC filter and the coupling inductance are given in Eq. (14) to Eq. (19) assuming that the voltage source inverter in the inverter-based DG unit produces the required voltage value $\left(v_i = v^*_i\right)$.

$$\dot{i}_{odi} = \frac{1}{L_c}\left(v_{odi} - v_{bdi} - r_c i_{odi}\right) + \omega i_{oqi} \qquad (14)$$

$$\dot{i}_{oqi} = \frac{1}{L_c}\left(v_{oqi} - v_{bqi} - r_c i_{oqi}\right) + \omega i_{odi} \qquad (15)$$

$$\dot{i}_{ldi} = \frac{1}{L_f}\left(v_{idi} - v_{odi} - r_f i_{ldi}\right) + \omega i_{lqi} \qquad (16)$$

$$\dot{i}_{lqi} = \frac{1}{L_f}\left(v_{iqi} - v_{oqi} - r_f i_{lqi}\right) - \omega i_{ldi} \qquad (17)$$

$$\dot{v}_{odi} = \frac{1}{C_f}\left(i_{ldi} - i_{odi}\right) + \omega v_{oqi} + R_d\left(\dot{i}_{ldi} - \dot{i}_{odi}\right) \qquad (18)$$

$$\dot{v}_{oqi} = \frac{1}{C_f}\left(i_{lqi} - i_{oqi}\right) - \omega v_{odi} + R_d\left(\dot{i}_{lqi} - \dot{i}_{oqi}\right) \qquad (19)$$

Here, v_i and v^*_i are the voltage and reference voltage on the AC side of the voltage source inverter bridge, respectively. The indices r_f and r_c are the parasitic resistance of the inductors L_f and L_c respectively. The resistor R_d is a damping resistor which is connected with the filter capacitor C_f in series form. The small signal complete linear state space model of an inverter-based DG unit is presented in Eq. (20) and Eq. (21),

which consists of the combination of small signal linearized state space models of the outer loop power dispatch controller, inner voltage and current controller and LCL output filter. In each model of the inverter-based DG unit, there are thirteen state variables, three inputs and two outputs (except for the first inverter-based DG unit, whose reference frame is the common reference frame, which has three outputs). In this regard, A_{IIDGi} represent the state matrix of ith inverter-based DG unit, B_{IIDGi} and B_{iwcom} are the input matrices of ith inverter-based DG unit which are related to the voltage and frequency inputs, respectively. The indices C_{IIDGi} and C_{IIDGwi} are the output matrices for ith inverter-based DG unit which are related to the output current (Δi_{oDQ}) and frequency ($\Delta \omega_i$), respectively. The state vector Δx_{IIDGi} includes the state space models of the external power dispatch controller, inner current and voltage controllers, and the output LCL filter which is characterized by a thirteen-element vector according to Eq. (22). Therefore, complete linear state space model of the small signal generation submodule was written by combining all the states of all inverter-based DG units n_g in the common reference frame according to Eq. (23) to Eq. (25). Also, according to Eq. (26) to Eq. (28), we will have as bellow.

$$\left[\Delta \dot{x}_{IIDGi} \right]_{13\times1} = \left[A_{IIDGi} \right]_{13\times13} \left[\Delta x_{IIDGi} \right]_{13\times1} + \left[B_{IIDGi} \right]_{13\times2} \left[\Delta v_{bDQi} \right]_{2\times1} \quad (20)$$
$$+ \left[B_{iwcom} \right]_{13\times1} \left[\Delta w_{com} \right]_{1\times1}$$

$$\begin{bmatrix} \Delta w_i \\ \Delta i_{oDQi} \end{bmatrix}_{3\times1} = \begin{bmatrix} \left[C_{IIDGwi} \right]_{1\times13} \\ \left[C_{IIDGi} \right]_{2\times13} \end{bmatrix}_{3\times13} \left[\Delta x_{IIDGi} \right]_{13\times1} \quad (21)$$

$$\Delta x_{IIDGi} = \begin{bmatrix} \Delta \delta_i & \Delta P_i & \Delta Q_i & \Delta \phi_{dqi} & \Delta \gamma_{dqi} & \Delta i_{ldqi} & \Delta v_{odqi} & \Delta i_{odqi} \end{bmatrix}^T \quad (22)$$

$$\left[\Delta \dot{x}_{GEN} \right]_{13n_g\times1} = \left[A_{GEN} \right]_{13n_g\times13n_g} \left[\Delta x_{GEN} \right]_{13n_g\times1} \quad (23)$$
$$+ \left[B_{GEN} \right]_{13n_g\times2n_g} \left[\Delta v_{bdq} \right]_{2n_g\times1} + \left[B_{GENw} \right]_{13n_g\times1} \left[\Delta w_{com} \right]_{1\times1}$$

$$\left[\Delta i_{oDQ} \right]_{2n_g\times1} = \left[C_{GENc} \right]_{2n_g\times13n_g} \left[\Delta x_{GEN} \right]_{13n_g\times1} \quad (24)$$

$$\left[\Delta w_{com} \right]_{1\times1} = \left[C_{GENw} \right]_{1\times13n_g} \left[\Delta x_{GEN} \right]_{13n_g\times1} \quad (25)$$

$$\Delta x_{GEN} = \begin{bmatrix} \Delta x_{IIDG1} \Delta x_{IIDG1} \cdots \Delta x_{IIDGn_g} \end{bmatrix}^T \quad (26)$$

$$\Delta v_{bDQ} = \begin{bmatrix} \Delta v_{bDQ1} \Delta v_{bDQ2} \cdots \Delta v_{bDQn_N} \end{bmatrix}^T \quad (27)$$

$$\Delta i_{oDQ} = \begin{bmatrix} \Delta i_{oDQ1} \Delta i_{oDQ2} \cdots \Delta i_{oDQn_g} \end{bmatrix}^T \quad (28)$$

In above relation, A_{GEN} is the state matrix for generation submodule, B_{GEN} and B_{GENw} are the input matrices for generation submodule which are related to

voltage and frequency inputs, respectively. The indices C_{GENc} and C_{GENw} are output matrices of the generation submodule which are related to current and frequency outputs, respectively.

2.2 Network Sub-Module

In the small signal modeling of a conventional power system, network dynamics are generally neglected due to the high time constant of rotating machines such as generators and synchronous motors and their control compared to the time constant of the network. However, in inverter-based MGs, inverter-based DG units are connected to each other through voltage source inverters that have a very small time constant. Due to the small time constant, network dynamics will have a significant effect on the MGs stability during off-grid operation mode. The dynamic equations of ith line between nodes j and k, shown in Fig. 4, are expressed in the common reference frame DQ according to Eq. (29) and Eq. (30). Eq. (31) and Eq. (32) represent the small signal linear state space model based on Eq. (29) and Eq. (30). Therefore, the linear state space model of the small signal network submodule with n_L lines can be expressed in the common reference frame based on Eq. (33) and Eq. (34).

Fig. 4 Configuration of line RL

$$\dot{i}_{lineDi} = -\frac{-R_{linei}}{L_{linei}} i_{lineDi} + \frac{1}{L_{linei}} \left(v_{bDj} - v_{bDk} \right) + \omega i_{lineQi} \quad (29)$$

$$\dot{i}_{lineQi} = \frac{-R_{linei}}{L_{linei}} i_{lineQi} + \frac{1}{L_{linei}} \left(v_{bQj} - v_{bQk} \right) - \omega i_{lineDi} \quad (30)$$

$$\dot{i}_{lineDi} = \frac{-R_{linei}}{L_{linei}} \Delta i_{lineDi} + \frac{1}{L_{linei}} \left(v_{bDj} - v_{bDk} \right) + I_{lineQi} \Delta \omega_{com} \quad (31)$$

$$\dot{i}_{lineQi} = \frac{-R_{linei}}{L_{linei}} \Delta i_{lineQi} + \frac{1}{L_{linei}} \left(v_{bQj} - v_{bQk} \right) + I_{lineDi} \Delta \omega_{com} \quad (32)$$

$$\left[\Delta \dot{i}_{LINEDQ} \right]_{2n_L\times1} = \left[A_{NET} \right]_{2n_L\times2n_L} \left[\Delta i_{LINEDQ} \right]_{2n_L\times1} \quad (33)$$
$$+ \left[B_{1NET} \right]_{2n_L\times2n_L} \left[\Delta v_{bDQ} \right]_{2n_N\times1} + \left[B_{2NET} \right]_{2n_L\times1} \left[\Delta w_{com} \right]_{1\times1}$$

$$\left[\Delta i_{LINEDQ} \right]_{2n_L\times1} = \left[C_{NET} \right]_{2n_L\times2n_L} \left[\Delta i_{LINEDQ} \right]_{2n_L\times1} \quad (34)$$

$$\Delta i_{LINEDQ} = \begin{bmatrix} \Delta i_{lineDQ1} \Delta i_{lineDQ2} \cdots \Delta i_{lineDQn_L} \end{bmatrix}^T \quad (35)$$

$$\Delta v_{bDQ} = \begin{bmatrix} \Delta v_{bDQ1} \Delta v_{bDQ2} \cdots \Delta v_{bDQn_N} \end{bmatrix}^T \quad (36)$$

In the above relationships, A_{NET} is the state matrix of the network submodule, B_{1NET} and B_{2NET} are the input matrices of the network submodule related to the input voltage and frequency.

2.3 Load Sub-Module

Different types of loads such as passive static loads such as resistive load (R), inductive load (RL), constant power load (CPL) and active loads and induction motor dynamic load are connected to inverter-based MGs. Here, it is assumed that dynamic and static loads are connected to the MG at the same time. The comprehensive small signal linear state space model for a load submodule is obtained by dividing it into three sub-modules including passive, active and dynamic. Inductive loads including electric motors, solenoid and toroid which can be modeled as RL type loads, may require very large starting power. Incandescent lamps, TV, radio, computer, laptop, and phone charger can be modeled as resistive load or DC load. Resistive load can also be modeled as a type of RL load with the assumption that its inductance value is very small. A constant power load (CPL) is a passive model of an active load with a rectifier interface (RIAL). In the CPL load, the instantaneous impedance value is always positive and the increasing value of the impedance is always negative, which cause to voltage decrement with the current increment and vice versa. This increasing negative impedance may lead to the instability of the inverter-based MG system during off-grid operation mode. Dynamic equations of ith passive load connected to the bus (n_N^{th}) shown in Fig. 5 based on the DQ reference frame are according to Eq. (37) and Eq. (38).
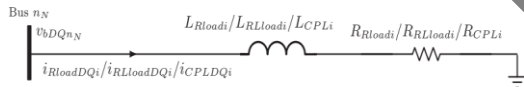
Fig. 5 Passive load configuration

The linearized state space model of ith passive load small signal connected to the node n_N^{th} in the common reference frame is given according to Eq. (39). Therefore, the linearized state-space model of a small-signal passive load submodule that includes the passive load n_{PL} in the common DQ reference frame is expressed as Eq. (40) and Eq. (41).

$$\dot{i}_{PLDi} = \frac{-R_{PLi}}{L_{PLi}} i_{PLDi} + \frac{1}{L_{PLi}} v_{bDnN} + \omega i_{PLQi} \tag{37}$$

$$\dot{i}_{PLQi} = \frac{-R_{PLi}}{L_{PLi}} i_{PLQi} + \frac{1}{L_{PLi}} v_{bQnN} - \omega i_{PLDi} \tag{38}$$

$$\left[\dot{\Delta i}_{PLDQi} \right]_{2\times1} = \left[A_{LOADi} \right]_{2\times2} \left[\Delta i_{PLDQi} \right]_{2\times1} \tag{39}$$
$$+ \left[B_{1LOADi} \right]_{2\times2} \left[\Delta v_{bDQn_N} \right]_{2\times1} + \left[B_{2LOADi} \right]_{2\times1} \left[\Delta w_{com} \right]_{1\times1}$$

$$\left[\dot{\Delta i}_{PLDQ} \right]_{2n_{PL}\times1} = \left[A_{PL} \right]_{2n_{PL}\times2n_{PL}} \left[\Delta i_{PLDQ} \right]_{2n_{PL}\times1} \tag{40}$$
$$+ \left[B_{1PL} \right]_{2n_{PL}\times2n_{PL}} \left[\Delta v_{bDQ} \right]_{2n_N\times1} + \left[B_{2PL} \right]_{2n_L\times1} \left[\Delta w_{com} \right]_{1\times1}$$

In these relationships, PL represents the passive loads R, RL and CPL. Also, $R_{CPL} = -r_{CPL}\cos\alpha$, $X_{CPL} = -r_{CPL}\sin\alpha$, and α is the delay angle of the controlled rectifier. The index A_{LOADi}, B_{1LOADi}, and B_{2LOADi} are the state and input matrices for ith passive load, which are related to the input voltage and frequency, respectively. In these above relationships, A_{PL} is the state matrix of the passive load submodule, B_{1PL} and B_{2PL} the input matrices of the passive load submodule are related to the voltage and frequency input respectively, the output of the passive load current is given in Eq. (42).

$$\left[\Delta i_{PLDQ} \right] = \left[\Delta i_{PLDQ1} \Delta i_{PLD2} \cdots \Delta i_{PLDQn_{PL}} \right]^T \tag{42}$$

Today, with advances in power electronics, more loads have active rectifiers. The power and active load control sections with the rectifier interface are shown in Fig. 6. The control section can be divided into the external DC voltage controller, which is the DC voltage of the capacitor (C_{dc}), and the internal AC current controller, which controls the current through the inductor (L_f). Fig. 7 shows DC voltage and AC current controllers of rectifier interfaced active load. These controllers are controlled by a standard PI controller. The DC voltage controller determines the reference input for the AC current controller, while the AC current controller controls the current through the L_{fAL} inductor.
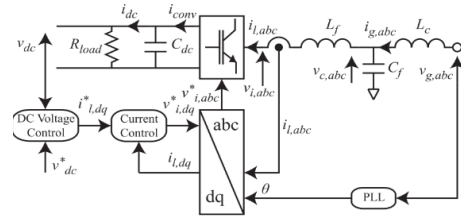

Fig. 6 The power and active load control sections with the rectifier interface
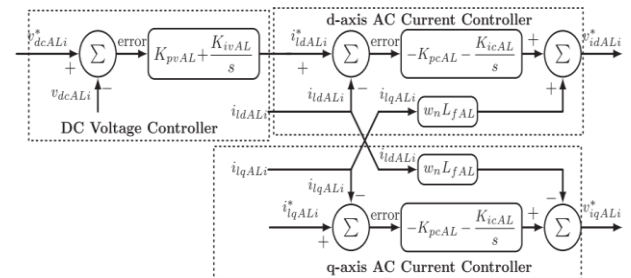

Fig. 7 DC voltage and AC current controllers of rectifier interfaced active load

In addition, the AC current controller uses the measured i_{ldqALi} for separation of DQ axis inductor currents. In this case, d and q axes are separated by multiplying the measured currents i_{ldqALi} with the system rated frequency (ω_n) and inductor (L_{fAL}), which is shown in Fig. 7. The small signal linear state space model of ith rectifier interfaced active load with the connected to the bus n_N^{th} in the DQ reference frame is given as Eq. (43) and Eq. (44). This model is obtained by combining state space models of DC voltage controllers and switching bridge AC current, LCL filter of AC section, DC load and reference frame coupling. This model has ten state variables including six inputs and three outputs. In these relationships, index A_{ALi} is the state matrix of ith rectifier interfaced active load. Indexes B_{ALvi}, B_{ALui} and B_{ALwi} as the input matrices of ith rectifier interfaced active load are related to the voltage, control and frequency inputs, respectively. The index C_{ALi} is the output matrix of ith active load with rectifier interface is related to the currents and DC voltage. It is modeled according to Eq. (45) and Eq. (46). The small signal linear state space model of the active load submodule in the common reference frame by combining all the states n_{AL} are given in Eq. (47) and Eq. (48).

$$\left[\Delta \dot{i}_{ALi}\right]_{10\times1} = \left[A_{ALi}\right]_{10\times10}\left[\Delta x_{ALi}\right]_{10\times1}$$
$$+\left[B_{ALui}\right]_{10\times2}\left[\Delta u_{ALi}\right]_{2\times1} + \left[B_{ALwi}\right]_{10\times1}\left[\Delta w_{com}\right]_{1\times1} \quad (43)$$

$$\left[\Delta y_{ALi}\right]_{3\times1} = \left[C_{ALi}\right]_{3\times10}\left[\Delta x_{ALi}\right]_{10\times1} \quad (44)$$

$$\Delta x_{ALi} = \begin{bmatrix} \Delta\phi_{Ali} & \Delta\gamma_{dqAli} & \Delta i_{ldqAli} & \Delta v_{cdqAli} & \Delta i_{gdqAli} & \Delta v_{dcAli} \end{bmatrix} \quad (45)$$

$$\Delta u_{ALi} = \begin{bmatrix} \Delta v_{dci}^* & \Delta i_{lqi}^* \end{bmatrix}^T \quad (46)$$

$$\left[\Delta \dot{x}_{AL}\right]_{10n_{AL}\times1} = \left[A_{AL}\right]_{10n_{AL}\times10n_{AL}}\left[\Delta x_{AL}\right]_{10n_{AL}\times1}$$
$$+\left[B_{ALv}\right]_{10n_{AL}\times2n_{AL}}\left[\Delta v_{bDQ}\right]_{2n_{AL}\times1} + \left[B_{ALu}\right]_{10n_{AL}\times2n_{AL}}\left[\Delta u_{AL}\right]_{2n_{AL}\times1}$$
$$+\left[B_{ALw}\right]_{10n_{AL}\times1}\left[\Delta w_{com}\right]_{1\times1} \quad (47)$$

$$\left[\Delta y_{AL}\right]_{3n_{AL}\times1} = \left[C_{AL}\right]_{3n_{AL}\times10n_{AL}}\left[\Delta x_{AL}\right]_{10n_{AL}\times1} \quad (48)$$

$$\left[\Delta x_{AL}\right] = \begin{bmatrix} \Delta x_{AL1}\Delta x_{AL2}\cdots\Delta x_{ALn_{AL}} \end{bmatrix}^T \quad (49)$$

$$\left[\Delta y_{AL}\right] = \begin{bmatrix} \Delta i_{ALDQ1}\Delta v_{DC1}\Delta i_{ALDQ2}\Delta v_{DC2}\cdots\Delta i_{ALDQn_{AL}}\Delta v_{DCn_{AL}} \end{bmatrix}^T \quad (50)$$

$$\left[\Delta u_{AL}\right] = \begin{bmatrix} \Delta u_{AL1}\Delta u_{AL2}\cdots\Delta u_{ALn_{AL}} \end{bmatrix}^T \quad (51)$$

In these relationships, index A_{AL} is the state matrix of the active load module. Indexes B_{ALv}, B_{ALu} and B_{ALw} are the input matrices related to voltage, control and frequency, respectively. Also, C_{AL} is the output matrix

for DC`s voltage and currents. Stator dynamic equations as well as electromagnetic dynamic equations and rotor load torque of ith induction motor (dynamic load) can be presented in the common DQ reference frame as follows:

$$v_{Qsi} = r_{si}i_{Qsi} + L_{ssi}\frac{di_{Qsi}}{dt} + L_{mi}\frac{di_{Qri}}{dt} + \omega L_{ssi}i_{Dsi} + \omega L_{mi}i_{Dri} \quad (52)$$

$$v_{Dsi} = r_{si}i_{Dsi} + L_{ssi}\frac{di_{Dsi}}{dt} + L_{mi}\frac{di_{Dri}}{dt} - \omega L_{ssi}i_{Qsi} - \omega L_{mi}i_{Qri} \quad (53)$$

$$v_{Qri} = r_{ri}i_{Qri} + L_{ri}\frac{di_{Qri}}{dt} + L_{mi}\frac{di_{Qsi}}{dt} + s_i\omega L_{mi}i_{Dri} + s_i\omega L_{mi}i_{Dsi} \quad (54)$$

$$v_{Dri} = r_{ri}i_{Dri} + L_{ri}\frac{di_{Dri}}{dt} + L_{mi}\frac{di_{Dsi}}{dt} - s_i\omega L_{mi}i_{Qri} - s_i\omega L_{mi}i_{Qsi} \quad (55)$$

$$T_{ei} = \left(\frac{3}{2}\right)\left(\frac{P_i}{2}\right)L_{m_i}\left(i_{Qsi}i_{Dri} - i_{Dsi}i_{Qri}\right) \quad (56)$$

$$T_{ei} - T_{Li} = J_i\frac{d}{dt}\left((1-s_i)\omega_i\right) \quad (57)$$

In these relationships, r_{si} and L_{ssi} are the resistance and inductance of the stator, as well as r_{ri} and L_{ri} are the resistance and inductance of the rotor for ith load of the induction motor. Indexes L_{mi}, s_i and ω_i are the dispersion inductance, rotor slip and stator angular frequency, respectively. In Eq. (56) and Eq. (57), P_i, T_{Li} and J_i are the number of poles, the load torque and the combination of the load and the motor inertia, respectively. It should be noted that in the inverter based MG system, the stator frequency is controlled by droop equations, and therefore, small signal deviations must be considered before linearizing the machine equations.

2.4 Diesel Generator Sub-Module

Droop control method can be used to control the performance of synchronous diesel generators in the MG, so that, in addition to adjusting the frequency and voltage in steady state, power redispatch can also be correctly guaranteed. Fig. 8 shows the implementation of the cooperative droop control for synchronous diesel generators in the MG.
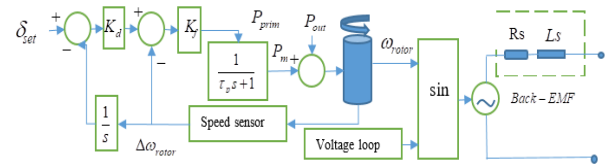

Fig. 8 Cooperative droop control for synchronous diesel generators in the MG

In the secondary control scheme, MG frequency and voltage changes are considered as functions of active power and voltage changes, respectively. The importance of the secondary control of the MG is sensed at the off-grid operation mode of MG because the

frequency and voltage of the system suffer a steady state drop over the time, which the primary control is not able to compensate these drops. This difference is shown in Fig. 9.
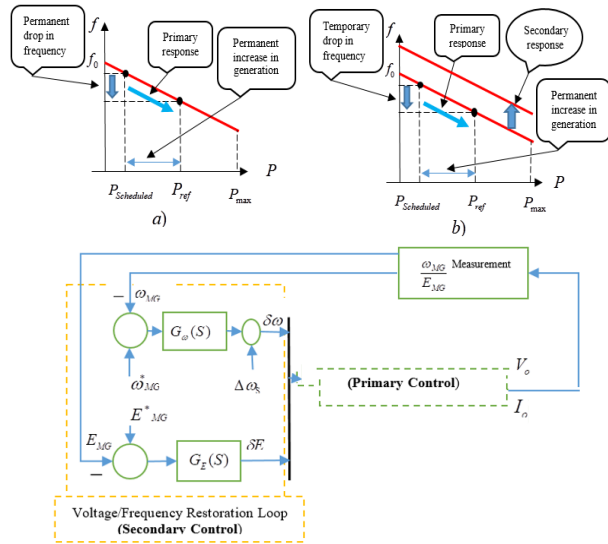

Fig. 9 Secondary control for off-grid MG

In the secondary control of an external loop, after measuring the frequency and voltage of the MG buses and calculating the frequency and voltage errors from the reference values, errors pass through a low-pass transfer function until these values have been used to calculate the frequency and voltage drops as primary control after synchronizing the frequency. The formulation of this method in which the PI controller is used to recover the frequency and voltage will be obtained from Eq. (58) and Eq. (59), respectively.

$$\delta\omega = k_{p\omega}(\omega_{MGs}^{*} - \omega_{MG}) + k_{i\omega}\int(\omega_{MGs}^{*} - \omega_{MG})dt + \Delta\omega_s \quad (58)$$

$$E = k_{pE}(E_{MGs}^{*} - E_{MG}) + k_{iE}\int(E_{MGs}^{*} - E_{MG})dt \quad (59)$$

3. Proposed Control Design

MGs often operate in on-grid and off-grid modes. In the on-grid operation mode, upstream network is responsible to control and maintain the MG frequency and voltage stability under various contingency events such as short circuit, load change and etc. But, in off-grid operation mode, MG frequency and voltage stability is controlled by use of inverter-based DG resources, controllable loads and also synchronous diesel generators. In our proposed approach, two level control processes are considered in the case of MG off-grid operation mode, the first level has very fast response again contingency events in order to maintain frequency and voltage stability that depend on proper operation of inverter-based DERs equipped with the power processing section and local control. The secondary level has slower response again contingency events depend on

the operation of the synchronous diesel generators and it is used to active and reactive power redispatch and remove the voltage and frequency offsets in MG system. The flowchart of overall performance of the MG adaptive control approach is shown in Fig. 10. To implement the proposed control flowchart, the dynamic modeling of the inverter-based MG system including static and dynamic loads and the rectifier interface adjustable load are investigated at the first level. The control scheme of synchronous DG resource is presented at the second level. Multi-level inverters (cascade bridge type) replacement with conventional inverter in inverter-based DERs is explained.
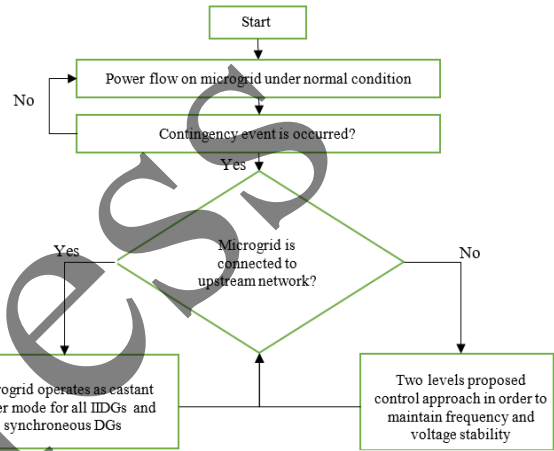
Fig. 10 Flowchart of overall performance of the MG adaptive control approach

In this section, the control scheme of multi-level cascaded bridge inverter is followed for replacement with conventional inverter in inverter-based DERs for improving the harmonic conditions of the MG. Therefore, first the structure of multi-level cascade bridge inverter is discussed and then, the optimal controller is proposed for this type of interface using genetic algorithm (GA). In the multi-level cascade bridge inverter, if the number of DC sources is P, then 2P-1 levels are created in each phase voltage waveform. For active power conversion, separate DC sources and no additional capacitors are required. Fig. 11 shows the structure of a three-level cascade bridge inverter. The main applications of the cascade multi-level inverter include the static generation of reactive power and creating a suitable interface between renewable energy resources. The most important advantages of the inverter-based multilevel inverters with cascade bridge structure are consisting of the modular structure, the problem elimination for equal voltage sharing for equipment with series connection. The possible numbers of levels in the output voltage is more than twice of DC sources. The bridge series are made for modular and

packaged arrangement, which causes to the faster production process and less investment cost. But, the disadvantage of the cascade structure is the need for a large number of isolated DC sources and a switching counter device. As described in section (2), the voltage and current controllers at the inner loop of the inverter-based DG resources, in addition to rejection of high frequency disturbances and providing sufficient damping for the filter output, are responsible for generating the filter reference current and reference voltage trough generating the pulse width modulation command for multi-level inverter in IIDGs. The measured voltage of IIDGs buses in MG after park conversion is applied to produce the error signal and compare with reference voltage produced by the inner loop current of IIDGs according to Eq. (60). After comparing and generating the voltage error signal for the mentioned busses in the reference frame dq, according to the Eq. (61) and Eq. (62), the calculated error value is returned from dq to $\alpha\beta$ space and $\alpha\beta$ to abc space by use of the inverse of Park and Clark transformations, respectively. Considering time domain error signal, comparing several carrier waves with the sinusoidal waveform (MCPDPWM) is used to generate the switching command pulse to the multi-level inverters of IIDGs. Fig. 12 shows the comparison of the carrier waves with frequency m-1 and main voltage wave for the positive and negative half-cycles at the above of the axis that the generated pulses results are sent to the desired switches. Standard proportional-integral (PI) regulators are used in local inner loop voltage-current controllers of each IIDG in MG to achieve the reference voltage.
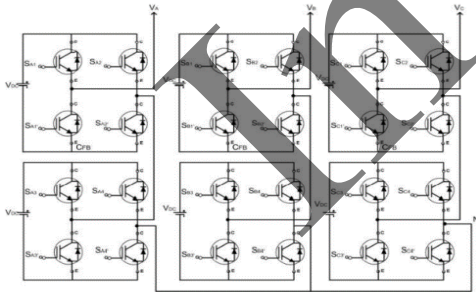
Fig. 11 Structure of a three-level cascade bridge inverter
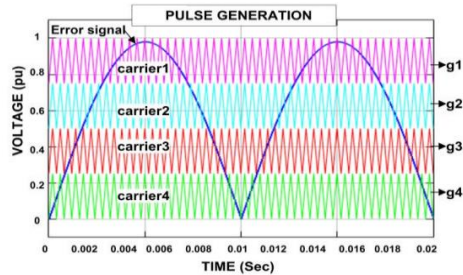
Fig. 12 Generated pulses results to send the switches of multi-level inverter

$$V_{DGi(error,dq)} = V_{DGi(ref,dq)} - V_{DGi(dq)} \qquad (60)$$

$$\begin{pmatrix} v_\alpha \\ v_\beta \end{pmatrix} = \begin{bmatrix} \cos wt & -\sin wt \\ \sin wt & \cos wt \end{bmatrix} \begin{pmatrix} v_d \\ v_q \end{pmatrix} \qquad (61)$$

$$\begin{pmatrix} v_\alpha \\ v_\beta \end{pmatrix} = \sqrt{\frac{2}{3}} \begin{bmatrix} 1 & -\dfrac{1}{2} & -\dfrac{1}{2} \\ 0 & \dfrac{\sqrt{3}}{2} & -\dfrac{\sqrt{3}}{2} \end{bmatrix} \begin{pmatrix} v_a \\ v_b \\ v_c \end{pmatrix} \qquad (62)$$

Standard integral (K_{pi}) and proportional (K_{ii}) gains, as well as feedforward (F_i) gains are the parameters of ith inner loop voltage-current controllers for IIDG as can be seen in Fig. 1. These parameters can be optimally determined for better dynamic performance of the MG using the GA. Therefore, the structure of the GA chromosomes with regard to the five mentioned independent variables is according to the Table. 1.

Table 1 Chromosomes structure based on standard integral and proportional and feedforward gains

K_{ii}	K_{pi}	K_{iv}	K_{pv}	F

For each chromosome of the initial population, the MG model is implemented using proposed control scheme during normal operation, and the level of each harmonic and total harmonic distortion is calculated for all the MG buses. Therefore, for solving the mentioned optimization problem, power quality improvement in addition to maintaining the MG frequency and voltage stability by use of the multi-level inverter has been considered. Therefore, the value of the fitness function in the GA is calculated based on proportional, integral and feedforward voltage regulator in inner current loop coefficients according to equation Eq. (63). The penalty values due to violations from the standard total harmonic distortion for the voltage wave in MG are imposed to the fitness function according to Eq. 64.

$$OF = Min\left(\sum_{Va,Vb,Vc} \left\{ \sum_{Bi=1}^{Nb} THD^{Bi}{}_{vi}(t) + Penalty^{Bi}{}_{chrom} \right\} \right) \qquad (63)$$

$$Penalty^{Bi}{}_{chrom} = \sum_{t=0}^{Ts} \left(\left| THD_{Vi}(t) - THD_{Vi}^{t\,arget}(t) \right| \times 10^{+3} \right) \qquad (64)$$

After calculating the chromosomes fitness, the chromosomes are sorted from the highest fitness to the lowest, and some of them enter the mating pool in pairs with the probability of Pc to generate new child chromosomes for the next iteration of the algorithm according to Table. 2. After crossover process and creating offspring from the pair of parental chromosomes, the mutation process occurs with a probability of pm in all the offspring, which is modelled as Table 3.

Table 2 The pair of parental chromosomes structure for creating offspring chromosomes

K_{ii}	K_{pi}	K_{iv}	K_{pv}	F
$K_{ii}"$	$K_{pi}"$	$K_{iv}"$	$K_{pv}"$	F"

$K_{ii}"$	$K_{pi}"$	K_{iv}	K_{pv}	F
$K_{ii}"$	$K_{pi}"$	$K_{iv}"$	K_{pv}	F

Table 3 The mutation process structure for the offspring chromosomes

$K_{ii}"$	$K_{pi}"$	K_{iv}	K_{pv}	F
$K_{ii}"$	$K_{pi}"$	$K_{iv}"$	K_{pv}	F

$K_{ii}"$	$K_{pi}"$	K_{iv}	$K_{pv}""$	F
$K_{ii}"$	$K_{pi}""$	$K_{iv}"$	K_{pv}	F

In the first iteration of the algorithm, after the population of mutated children is formed then all the chromosomes are sorted based on their fitness. After that the number of the predetermined population similar to the first iteration is selected again from the chromosomes of parents and children until the next iteration of the algorithm is done. This process is repeated until the algorithm gets to the convergence condition i.e. the minimum amount of total harmonic distortion without violating the power quality standard for under study MG. Therefore, by adjusting these coefficients, it can be ensured that the MG by using the proposed control on IIDGs not only guarantees the frequency and voltage stability and zero offset synchronous DGs after occurrence of random events, but also improves the harmonic conditions for the buses of MG.

4. Simulation Results

In order to validate and confirm the effectiveness the proposed two-level control method with the aim of stability and power quality improvement of MG, numerical studies are performed on the test MG according to Fig. 13. As can be seen from the figure, under study MG includes four inverter interfaced DG resources. This MG is connected to the main distribution network through a tie switch and 100kVA step-up transformer with turn ratio of 415V/11kV at the point of common coupling (PCC). MG can operate in off-grid state when tie switch is open. The MG will operate nominal voltage and frequency 230V and 50 Hz, respectively. The nominal active and reactive powers of IIDG1, IIDG2, IIDG3 and IIDG4 are 10kw + j6kvar, 15kw + j9kvar, 20kw + j12kvar and 25kw + j15kvar, respectively. The static droop gain of the active power in term of radian/sec.watt for the inverter-based DERs include m_{P1}, m_{P2}, m_{P3} and m_{P4} are 6.28×10^{-4}, 4.18×10^{-4}, 3.14×10^{-4} and 2.52×10^{-4}, respectively. The static droop gain of the reactive power in term of

Volt/Var for the inverter interfaced DERs include n_{P1}, n_{P2}, n_{P3} and n_{P4} are 1.66×10^{-3}, 1.11×10^{-3}, 8.33×10^{-4} and 6.66×10^{-4}, respectively.
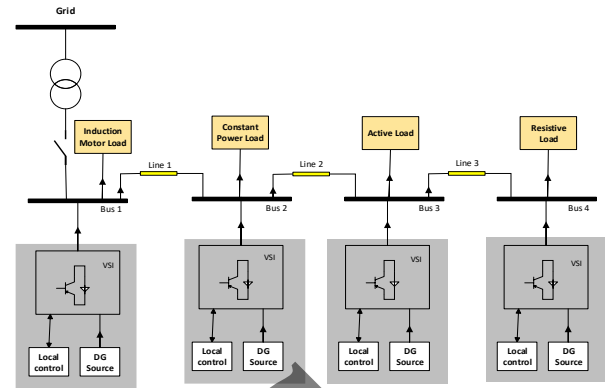
Fig. 13 MG structure in off-grid operation state

The output LC filter parameters of inverter-based DERs such as L_f, C_f and R_f are equivalent to 1.35mH, 50μF and 0.1Ω, respectively. The inverter switching frequency f_{sw} is equal to 8kHz. The cut-off frequency of the output low-pass filter is 31.41rad/s, the nominal frequency of the output voltage waveform of the inverter-based DG sources is equal to 50.5Hz. The resistance and inductance of the output inductor of inverter-based DERs are equal to 0.03Ω and 0.35mH, respectively. The impedance of the Line1, Line2 and Line3 in the under study MG with off-grid operation are equal to (0.23+j0.11) Ω, (0.35+j0.58) Ω, and (0.30+j0.47) Ω, respectively. According to the Fig. 13, the load1 as an induction motor is connected to bus1 with technical specifications of 400 volts, 50 Hz and 7.5 kilowatts. Stator resistance r_s and inductance L_{ss} are equal to 0.7834Ω and 127.1mH respectively, rotor side resistance r_r and inductance L_{rr} are equal to 0.7402Ω and 127.1mH, respectively. The magnetization inductance L_m is equal to 124.1mH and the load torque T_L is equal to 47.75 Nm. The parameters of load2 as a constant power load at the bus2 include a resistance, power consumption and a power factor 13.224 Ω/phase, 12 kVA and 0.85, respectively. The characteristics of the active load with the rectified interface at bus3 are shown in Table. 4.

Table. 4 The characteristics of the active load with the rectified interface at bus3

R_f	0.1 Ω	L_f	1.35 mH
f_{sw}	10 kHz	C_f	8.8 μF
L_c	0.93 mH	K_{ii}	**25000**
Power	25kW	R_c	0.03 Ω

K_{iv}	150	w_c	31.41 rad/s
K_{pi}	7	K_{pv}	0.5
R_{RIAL}	40.833 Ω	R_{RLoad}	6.347 Ω/phase
–	–	V_{DC}	700 V

The power consumption, resistance per phase and nominal voltage specifications for the resistive load at bus4 are 25kw 6.347ohm and 700v, respectively. According to the given information, numerical studies are evaluated for two case studies as bellow:

- Case study1: normal operating condition for off-grid inverter-based MG.
- Case study2: fault occurrence event condition at bus2 with 1Ω resistance.

The GA parameters for number of iteration, population, crossover, and mutation probability are defined as 200, 1000, 0.7 and 0.3, respectively. The proposed model is implemented with the M-file format in the MATLAB software environment, this software is installed on a 5-core Asus Laptop with 2.4GHz processor and 500GB external memory.

4.1 Case1: Normal Operating Condition for off-grid Inverter-Based MG

The proposed dynamic model is used to study the performance of off-grid MG under normal operating conditions for 0.5 seconds. The internal voltage-current loop coefficients of inverter-based DERs and control system feedforward coefficient has been optimally determined using the GA as shown in Table. 5.

Table. 5 Internal voltage-current loop coefficients of inverter-based DERs and feedforward coefficients (case1)

K_{pv}	K_{iv}	K_{pi}	K_{ii}	F
0.05	390	10.5	16000	0.75

The active and reactive powers of DG resources, their operating frequency are shown in Fig. 14 and Fig. 15, respectively. It can be seen that the active power generations of IIDG1 to IIDG4 after passing system transient fluctuations are fixed at 0.64 kW, 3.45 kW, 44.09 kW and 24.54 kW, respectively. Their reactive power generations are fixed at 0.79 kvar, -1.76 kvar, 4.82 kvar and 11.89 kvar, respectively. The operating frequencies of IIDG1 to IIDG4 are also given in Fig. 16 that after passing transient fluctuations, these frequencies are fixed at 49.94 Hz, 49.88 Hz, 49.62 Hz and 49.72 Hz, respectively, that all these frequencies are considered within the permissible range of frequency changes in the power system.
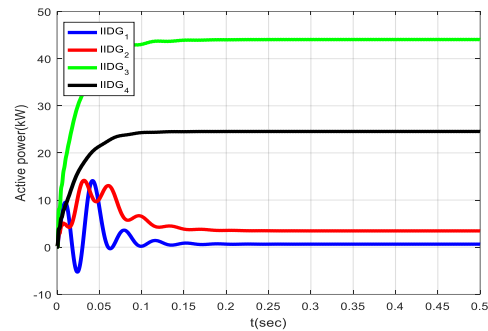
Fig. 14 Active power generation of IIDG1 to IIDG4 in off-grid MG (case1)
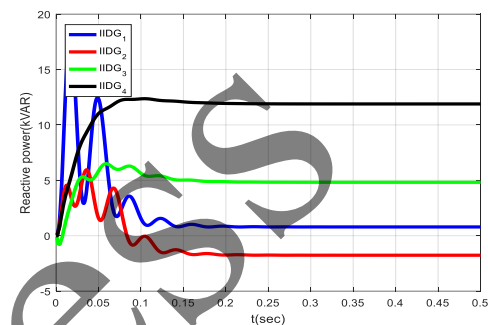
Fig. 15 Reactive power generation of IIDG1 to IIDG4 in off-grid MG (case1)
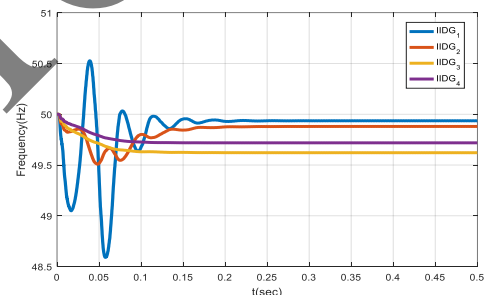
Fig. 16 Operating frequencies of IIDG1 to IIDG4 in off-grid MG (case1)
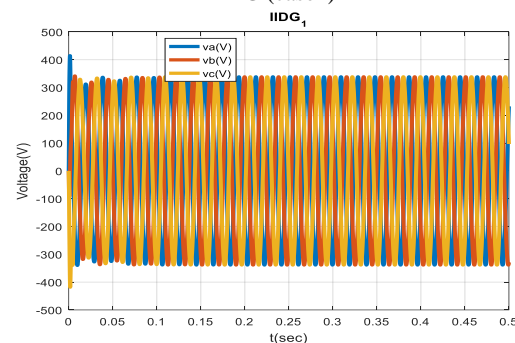
Fig. 17 Voltage of IIDG1 in off-grid MG (case1)
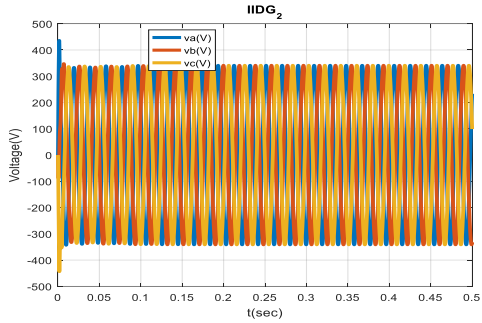
Fig. 18 Voltage of IIDG2 in off-grid MG (case1)
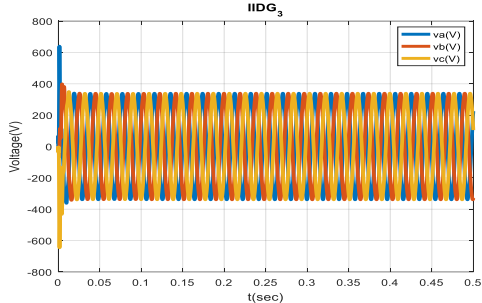
Fig. 19 Voltage of IIDG3 in off-grid MG (case1)
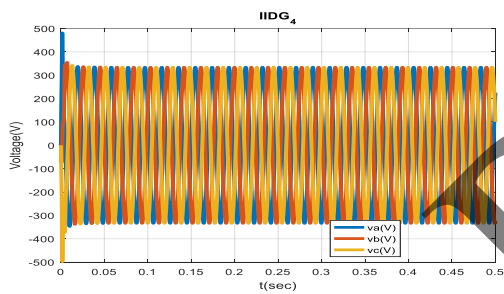
Fig. 20 Voltage of IIDG4 in off-grid MG (case1)

The three-phase voltage waveform for the inverter-based DERs are shown in Fig. (17) to Fig. (20), respectively. It can be seen that the three-phase voltage at the point of common coupling becomes completely sinusoidal waveform after passing through the transient state, and the magnitude of the output voltage of IIDG1 to IIDG4 are fixed at 338.6 V, 341.5 V, 339.4 V and 333.5 V, respectively. The three-phase current of IIDG1 to IIDG4 is shown in Fig. 21.
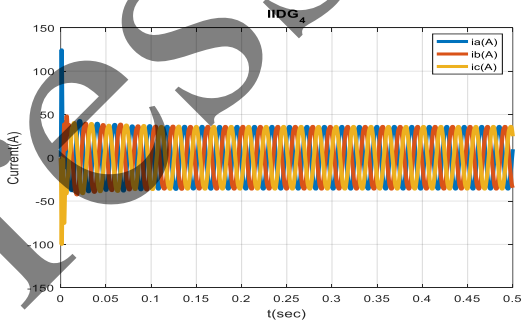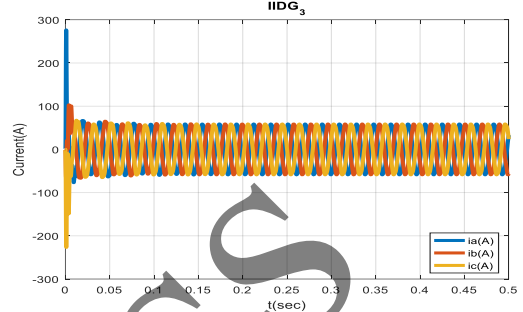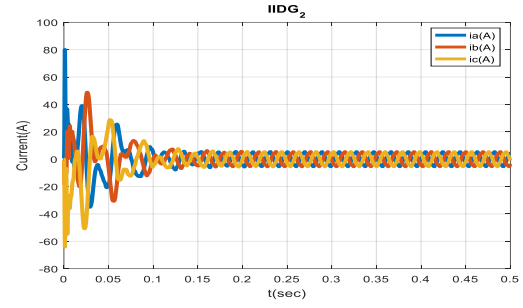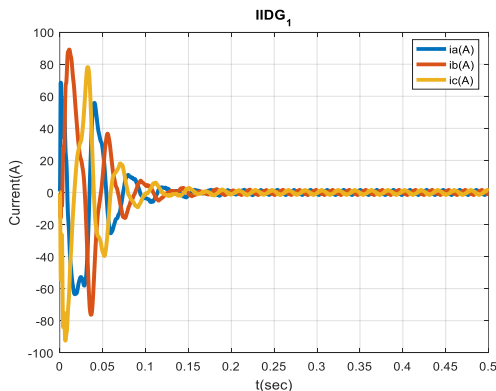
Fig. 21 The currents of IIDG1 to IIDG4 in off-grid MG (case1)

After significant non-sinusoidal fluctuations, three-phase currents of IIDG1 are fixed 1.64A at the connection point with the induction motor load, but, due to the presence of the active load at bus3, the currents of this source will have some order of harmonics. After severe fluctuations for steady state, three-phase currents of IIDG2 are fixed at 5.53A at the connection point with the constant power load, similar to IIDG1 source includes some order of harmonic. After small fluctuations in a very short period of time, three phase currents of IIDG3 for the steady state condition are fixed 58.83A at connection point with the rectified active load. Similar to the IIDG1 and IIDG2 resources, currents of IIDG3 have infected with harmonics but their values are much less than the two mentioned resources. After small fluctuations in a very short period of time, three phase current of IIDG4 has been fixed at 36.3A at connection point with the resistive load, and of course, the output currents of this source have much less harmonic than the other three inverter-based DERs. The D-axis voltages for inverter-based DERs are shown in Fig. 22 and the current of the three lines in the direction of D-axis and Q-axis are shown in Fig. 23 and Fig. 24, respectively. The three-phase stator currents of the induction motor at

bus1 is shown in Fig. 25 while this consumer draws a current equal to 13.38A in steady state condition after drawing a start-up currents equal to 128.3A.
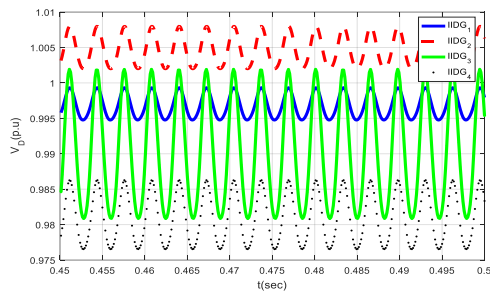
Fig. 22 Three-phase voltage of IIDGs in MG (P.U.) (case1)
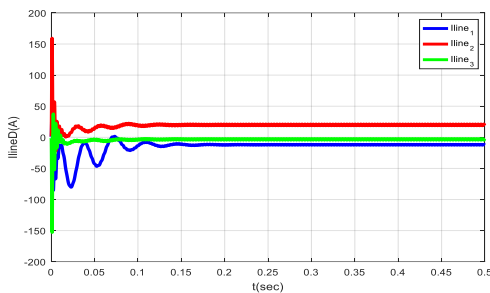
Fig. 23 D-axis current of lines between IIDG in MG (case1)
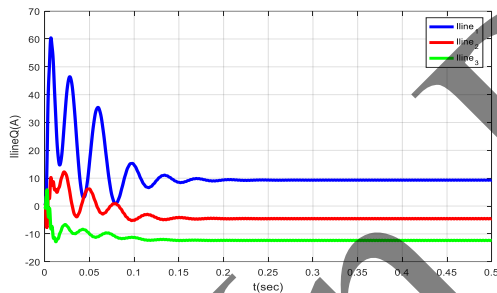
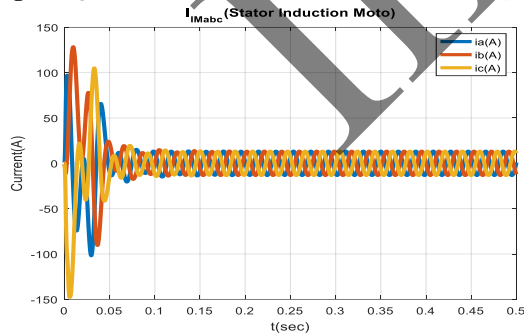
Fig. 24 Q-axis current of lines between IIDG in MG (case1)

Fig. 25 Three-phase stator current of Induction Machine load at bus1 in MG (case1)

The speed and electromagnetic torque characteristics for the induction motor load at bus1 in the under study MG are shown in Fig. 26 and Fig. 27, respectively.
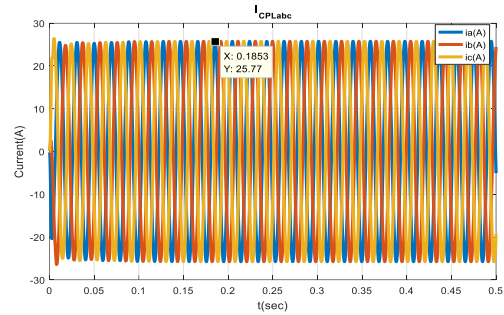
Fig. 28 Three-phase current of constant power load at bus2 (case1)
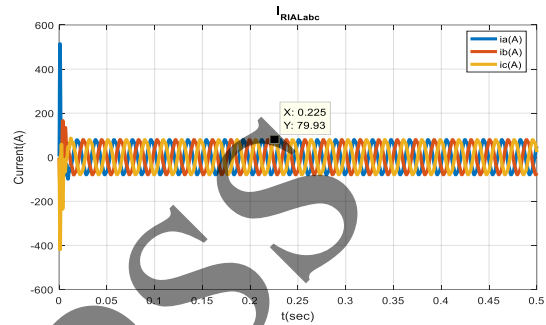
Fig. 29 Three-phase current of RIAL at bus3 (case1)
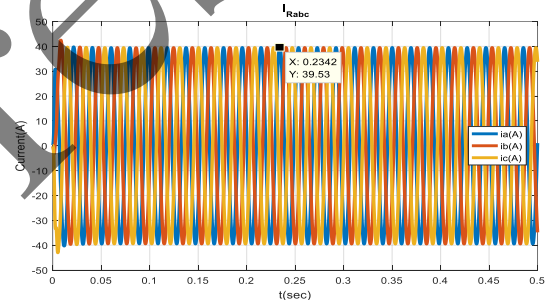
Fig. 30 Three-phase current of resistive load at bus4 (case1)

As can be seen from the above current waveforms, after passing the transient state, the magnitude of currents drawn by the active rectified and the resistive loads are equal to 79.93A and 39.53A, respectively. The voltage and power waveforms for rectified active load are also shown in Fig. 31 and Fig. 32, respectively.
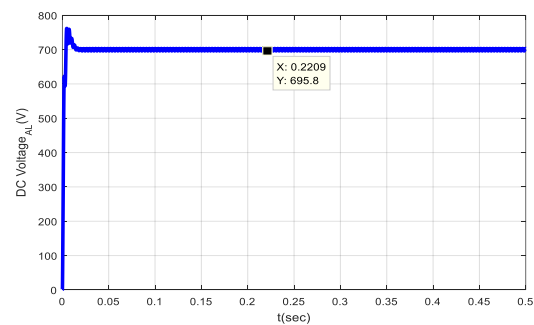
Fig. 31 Voltage magnitude of RIAL at bus3 (case1)
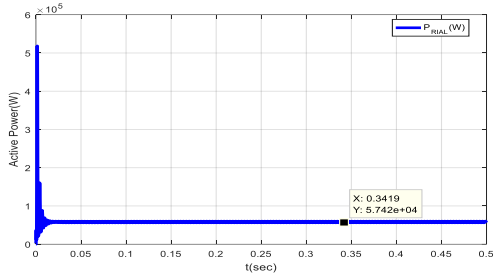
Fig. 32 Consumption power of RIAL at bus3 (case1)

As can be seen from the above figures, due to the switching losses of the rectifier, the power consumption and DC voltage magnitude at the terminal of rectified active load in steady state are equal to 695.8 volts and 57.42 kilowatts, respectively. As mentioned in the section (3), in addition to the frequency stability for the MGs based on inverter interfaced DERs, the proposed control approach ensures the improvement of harmonic conditions during island operation under normal conditions and random events by replacing multi-level inverters instead of the usual two-level ones. The simulation results for harmonics and total harmonic distortion of voltage waveform in phase-A at Bus1 under normal off-grid conditions of MG with DERs equipped with two-level inverters during time period 0.5 seconds are determined as shown in Fig. (33a) and (33b). By replacing the two-level inverters with three-level inverters in DERs, performance of MGs under normal off-grid conditions during time period 0.5 seconds has been re-determined which is shown in Fig. (34a) and (34b), respectively.

a) Harmonics of voltage waveform in phase A at Bus1

b) Total harmonic distortion of voltage waveform in phase A at Bus1

Fig. 33 simulation results for off-grid conditions of MG with DERs equipped with two-level inverters
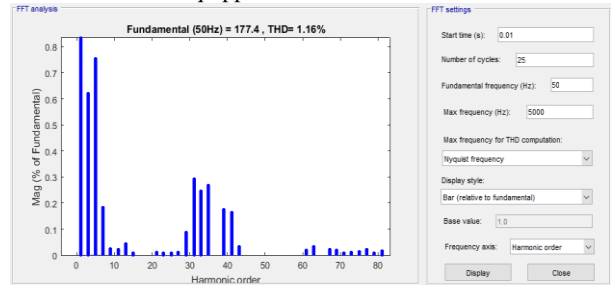
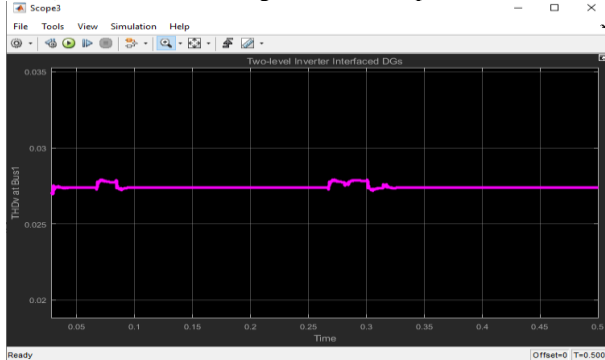
a) Harmonics of voltage waveform in phase A at Bus1
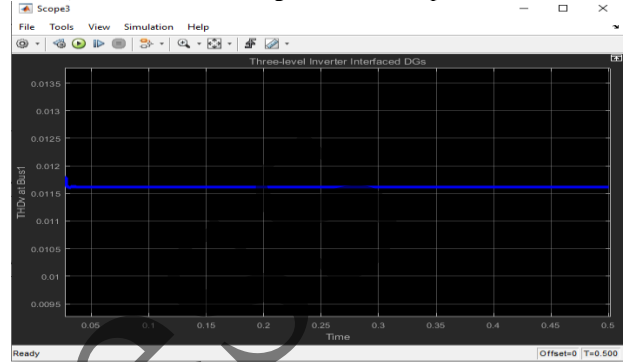
b) Total harmonic distortion of voltage waveform in phase A at Bus1

Fig. 34 simulation results for off-grid conditions of MG with DERs equipped with three-level inverters

From the above figures, it can be seen that the total harmonic distortion for DERs equipped with two-level and three-level inverters during the simulation period are determined by fix values 2.75% and 1.16%, respectively. By replacing the three-level inverters with two-level ones in DERs, the total harmonic distortion in phase-A at Bus1 is reduced from 2.75% to 1.16%. A significant change can be seen in the order of harmonics, while the magnitude of harmonics has dropped drastically. Of course, it is necessary to state that in the design phase of MGs, the increase in costs due to the installation of multi-level inverters for DERs should be evaluated according to the amount of reduction in the total harmonic distortion index for the buses voltages.
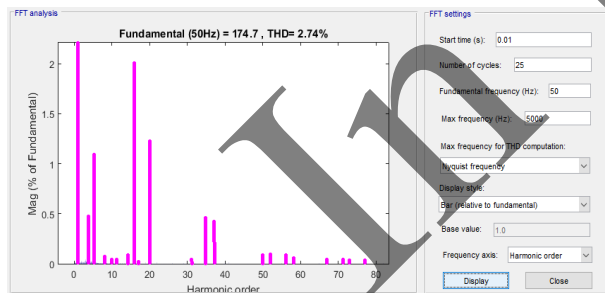
4.2 Case2: Fault Occurrence Event Condition at Bus2 with 1Ω Resistance

In this case study, it is assumed that a short circuit event with resistance 1Ω is occurred at bus2 and numerical results are evaluated for the response of off-grid MG during 0.2 seconds to 0.3 seconds using the proposed dynamic model.

Table. 5 Internal voltage-current loop coefficients of inverter-based DERs and feedforward coefficient (case2)

K_{pv}	K_{iv}	K_{pi}	K_{ii}	F
0.82	15500	9.5	425	0.03

With the fault occurrence at bus2, it is expected that

active and reactive power generation with IIDG2 will significantly increase, and of course, the contribution of other resources will also increase for current injection to fault location. After running the model, active and reactive power results of IIDG1 to IIDG4 and their operating frequency under the new conditions are shown in Fig. 35 to Fig. 37, respectively.
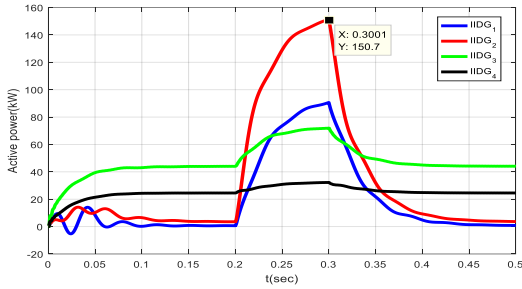

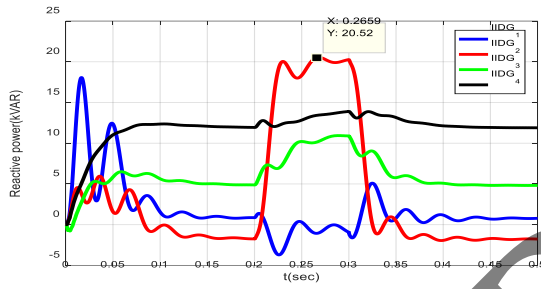**Fig. 35** Active power generation of IIDG1 to IIDG4 in off-grid MG (case2)

Fig. 36 Reactive power generation of IIDG1 to IIDG4 in off-grid MG (case2)
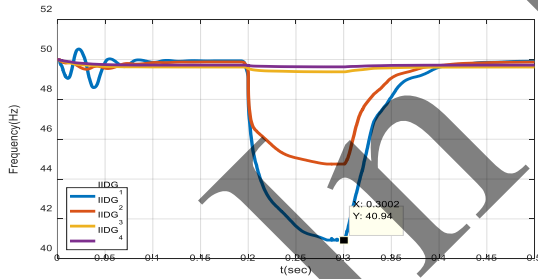
Fig. 37 Operating frequencies of IIDG1 to IIDG4 in off-grid MG (case2)

From the simulation results, it can be seen that the active power generation of IIDG1 to IIDG4 have increased during fault occurrence. For IIDG2, active power generation increases to 150.7 kW. Of course, the increase in the reactive power generation in IIDGs resources is evident, especially the IIDG2 whose reactive power generation reaches to 20.52 kvar. As can be seen in the Fig. 38, the frequencies of IIDG3 and IIDG4 have approximately remained constant and the frequencies of IIDG1 and IIDG2 get to 40.94Hz and 44.98Hz during fault occurrence according to the droopy curve. After fault clearing, frequencies of IIDG1 to IIDG4 have fixed in the values of 49.94 Hz, 49.88Hz, 49.62Hz and 49.72Hz, respectively. All these frequency

changes are within allowable range in the power system. The simulation results for the three-phase voltage waveform of IIDG resources under the new condition of short circuit occurrence in bus2 during 0.2 to 0.3 seconds are shown in Fig. 39.
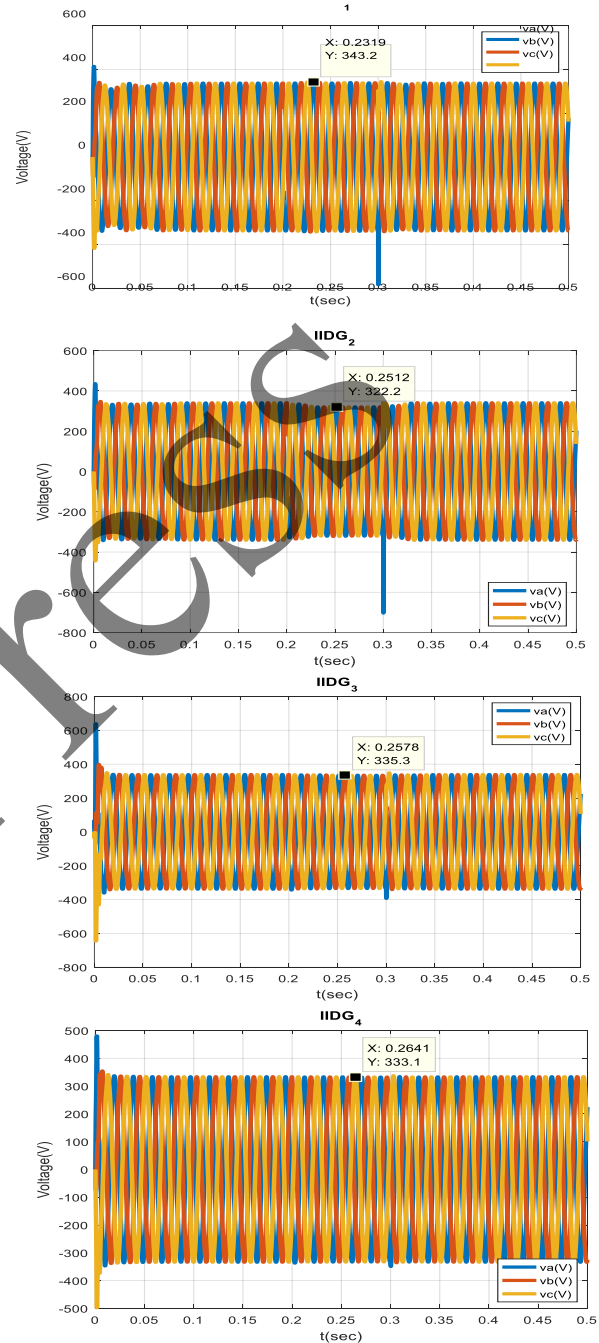

Fig. 39 Three-phase current IIDG1 to IIDG4 when three-phase fault occurrence at Bus2

After three-phase short circuit at bus2, the three-phase voltage at the connection point of the IIDGs with the MG is sinusoidal and the magnitude of the output voltage of the IIDG2 is only reduced to 322.2 volts.
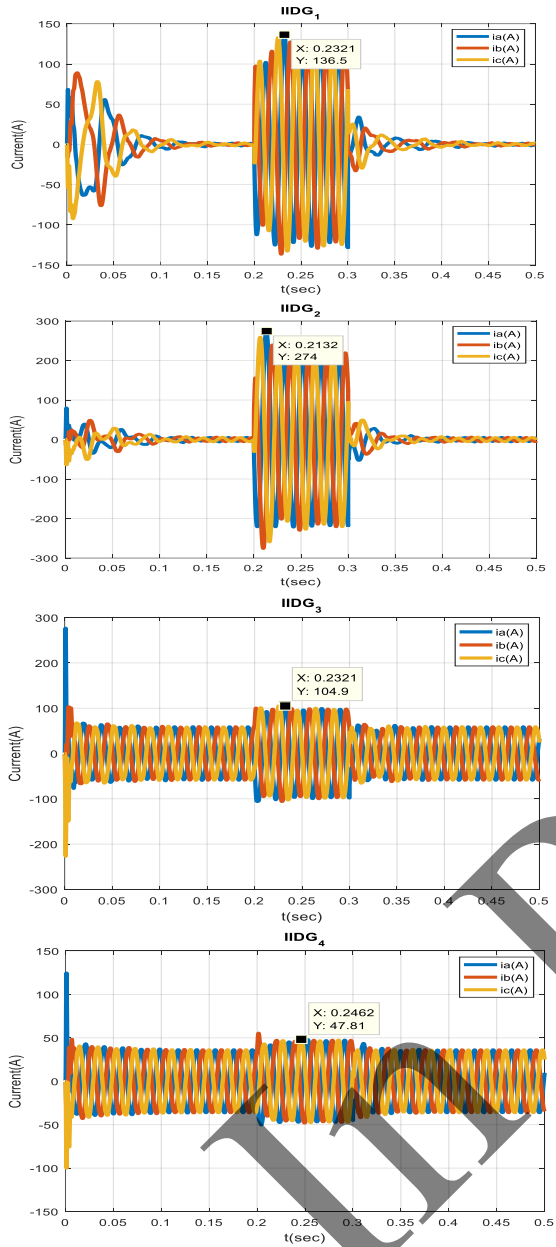
Fig. 39 Three-phase current IIDG1 to IIDG4 when three-phase fault occurrence at Bus2

As can be seen in the Fig. 39 the three-phase currents of IIDG1 to IIDG4 during the three-phase short circuit at bus2 increase to the values of 136.5A, 274A, 104.9A and 47.81A, respectively and after the fault clearance return to nominal values. The three-phase current waveforms of the IIDG resources are shown in Fig. 40. Under new condition, three-phase voltage of IIDGs in MG in term of per unit and Q-axis and D-axis currents of lines between IIDG in off-grid MG have been shown in Fig. 41 and Fig. 42, respectively.
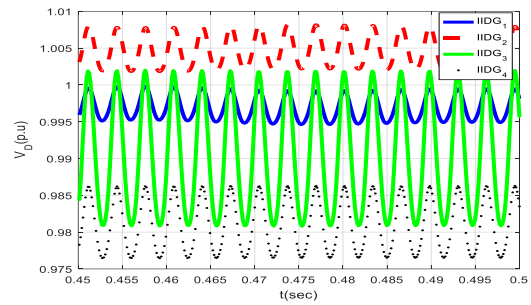
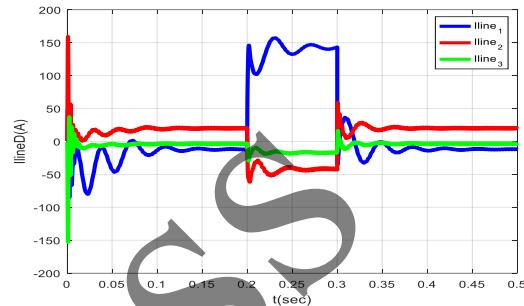**Fig. 40** Three-phase voltage of IIDGs in MG (P.U.) (case2)

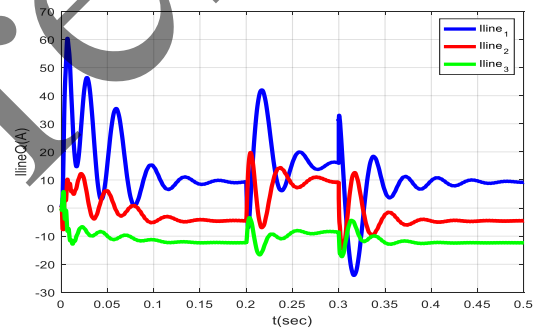**Fig. 41** D-axis current of lines between IIDG in off-grid MG (case2)

Fig. 42 Q-axis current of lines between IIDG in off-grid MG (case2)

As can be seen from Fig. 40 when a three-phase short circuit occurs at bus 2, magnitude of stator current of induction machine increases to 19.9A from 13.38A in steady state condition.
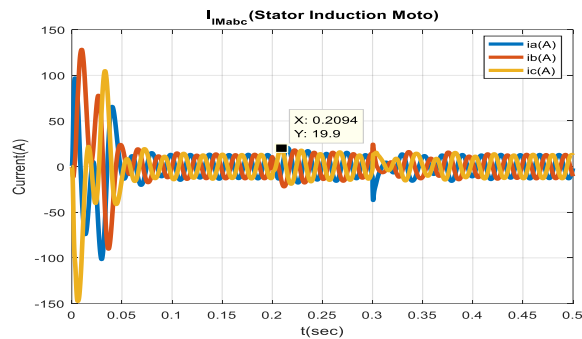

Fig. 43 Three phase stator current of induction machine load at Bus1 (case2)

Under the new condition of three-phase short circuit at bus 2, the characteristics of speed and electromagnetic

torque for the induction motor load connected to bus1 are shown in Fig. 44 and Fig. 45, respectively.
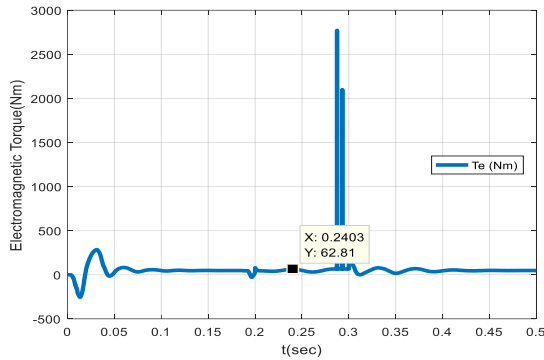

Fig. 44 Electromagnetic torque characteristic of Induction Machine load at Bus1 (case2)
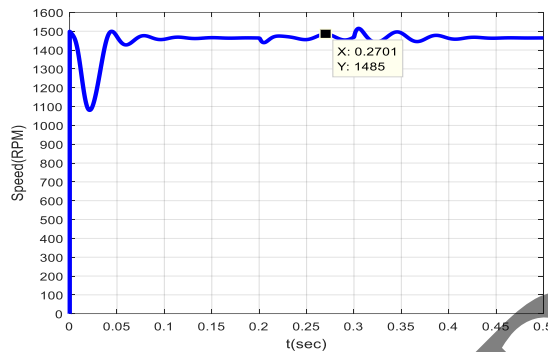

Fig. 45 Speed characteristic of Induction Machine load at Bus1 (case2)

As can be seen from Fig. 44 to Fig. 45 similar to case1, both electromagnetic torque and the speed characteristics of induction motor load after passing through the transient time interval, their fluctuations are damped and fixed at 47.7Nm and 1465rpm, respectively. When, a three-phase short circuit occurs at bus2, both of the mentioned variables undergo fluctuations, which return to their nominal values after removing the fault. Magnitude of electromagnetic torque and speed fluctuations are high and very low, respectively. According to Fig. 43, The magnitude of three-phase current for the constant power load connected to bus2 is 25.77A in steady state and have not any harmonics, but this current decreases to 24.21A when short circuit is occurred. The three-phase current waveform of the rectified active load and the resistive load connected to buses 3 and 4 of under study MG during three-phase short circuit event at bus2 are shown in Fig. 46 to Fig. 48, respectively. As can be seen from Fig. 43 to Fig. 45, the currents drawn by the active and resistive load connected to buses 3 and 4 during the short circuit event remain unchanged. Power consumption of the rectified active load in presence of occurrence of the three-phase short circuit at bus2 is shown in Fig. 49.
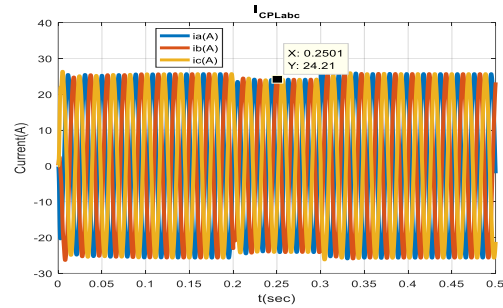

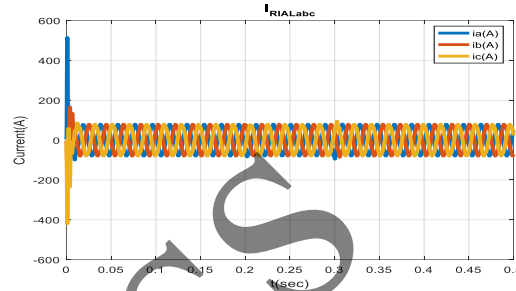**Fig. 46** Three-phase current for constant power load at Bus2

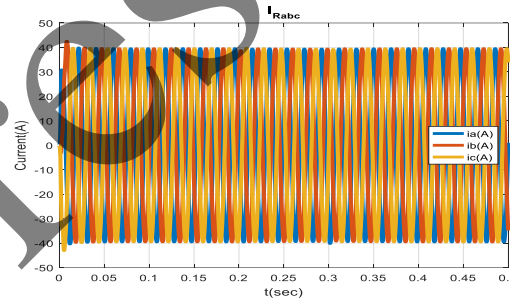**Fig. 47** Three-phase current for active load at Bus3

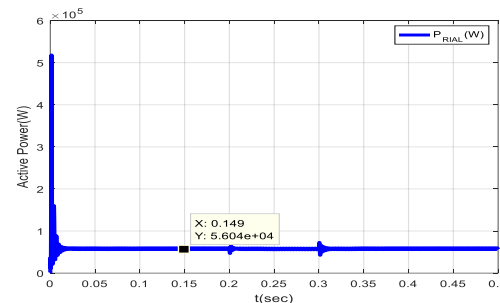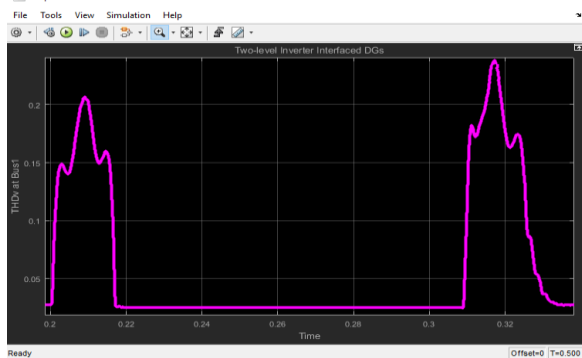**Fig. 48** Three-phase current for resistive load at Bus4

Fig. 49 Power consumption of the rectified active load in steady state in presence of occurrence of the three-phase short circuit at Bus2

As can be seen from Fig. 49, the power consumption and DC terminal voltage of the rectified active load is similar to case1 in presence of occurrence of the three-phase short circuit at bus2. The simulation results for harmonics and total harmonic distortion of voltage waveform in phase-A at Bus1 under normal off-grid conditions of MG with DERs equipped with two-level inverters are determined as shown in Fig. (50a) and (50b). For case2, it is assumed that three-phase fault is occurred between 0.2 second to 0.3 second during simulation time 0.5 seconds. Under same condition,

harmonics and total harmonic distortion of voltage waveform in phase-A at Bus1 has been determined in Fig. (51a) and (51b), respectively.
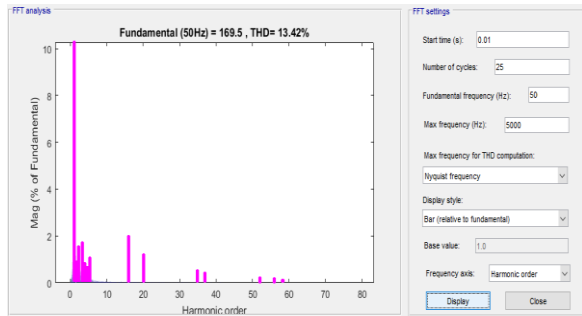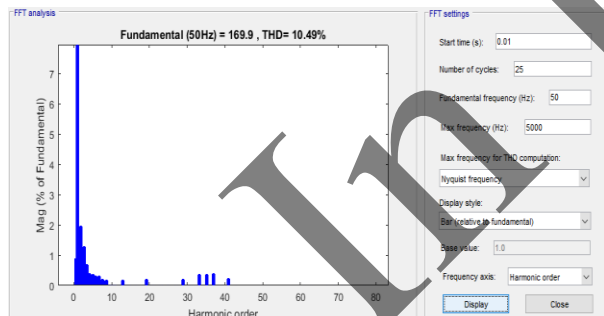

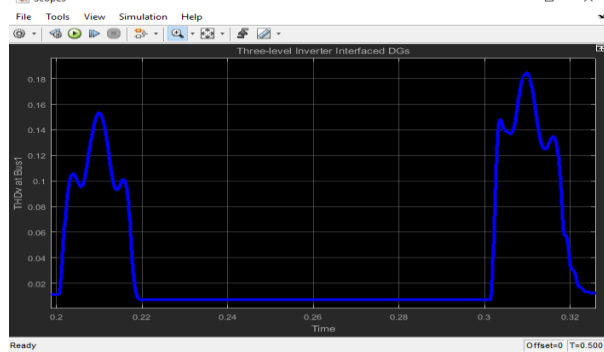a) a) Harmonics of voltage waveform in phase A at Bus1

b) b) Total harmonic distortion of voltage waveform in phase A at Bus1

Fig. 50 Results for off-grid MG with DERs equipped with two-level inverters under 3-phase fault condition

a) Harmonics of voltage waveform in phase A at Bus1

b) Total harmonic distortion of voltage waveform in phase A at Bus1

Fig. 51 Results for off-grid MG with DERs equipped with three-level inverters under 3-phase fault condition

As can be seen from the above figures, the fault occurrence and clearing causes an increase in the distortion in the voltage waveform at bus1, transiently, which leads to an increase in the amplitude of the harmonics and also the total harmonic distortion from 2.74% to 13.2% in the presence of two-level inverter based DERs and from 1.16% to 10.49% in the presence of three-level inverter based DERs, respectively. Therefore, it can be concluded that the use of DERs equipped with multi-level inverters provide a higher ability to reduce the harmonic level and total harmonic distortion of the MGs during normal and contingency events such as short circuit, and etc.

5. Conclusion

In this article, a two-level control approach is proposed to improve the stability and power quality of MGs. A dynamic model of MG is carried out using state space equations. At the first level, internal voltage and current control loop, local power distribution loop and power processing section are applied to control the inverter-based DERs. Then, a control scheme at the secondary level, synchronous diesel generators are used to achieve the minimum voltage and frequency offset in the MG. To improve the harmonic conditions in the MG, ordinary inverters are replaced with cascade bridge type multi-level inverters in the inverter-based DERs and switching command are optimized with the internal current loop coefficients of the reference voltage regulator using GA. Finally, in order to validate the efficiency of the proposed dynamic model and control scheme for the MG in off-grid operation state, numerical studies on a test MG have been investigated under normal operating conditions and three-phase short circuit occurrence. In the test MG, different types of loads including constant power load, active rectified and resistive loads and etc were studied, and their effect on the bus voltage magnitude of the MG, the amount of active and reactive power generation of DG resources and the amount of power consumption by the loads have been considered. The simulation results prove the fact that the proposed dynamic model and proposed control scheme for the MG can maintain the frequency stability under normal conditions and short circuit events, and dispatch the local load demand on inverter-based DERs and adjust the controllable load consumption. From simulation results, it can be seen that replacing the three-level inverters with two-level ones in DERs cause to decrease from 2.75% to 1.16% in the total harmonic distortion in phase-A at Bus1. In addition, the order of harmonics has changed and their magnitude dropped drastically. Fault

occurrence and clearing result in the total harmonic distortion increment in the voltage, transiently, from 2.74% to 13.2% in the presence of two-level inverter based DERs and from 1.16% to 10.49% in the presence of three-level inverter based DERs, respectively. Therefore, it can be concluded that the use of DERs equipped with multi-level inverters provide a higher ability to reduce the harmonic level and total harmonic distortion of the MGs during normal and contingency events such as short circuit, and etc. Of course, it is noted that the total harmonic distortion reduction for the buses voltages causes to increase in planning costs of MGs due to the installation of multi-level inverters for DERs, which should be considered using cost-benefit analysis.

References

[1] Chabok B.S., Sadegh Samiei M., Jalilvand A., and Bagheri A., "A Risk-Based Model for Reconfigurable Active Distribution Networks Scheduling in the Presence of Demand-Side Responsive Loads", 28th International Electrical Power Distribution Conference (EPDC), IEEE, pp.1-10, 2024, DOI:10.1109/EPDC62178.2024.10571760.

[2] Abedi T., Yousefi G. and Shafie-khah M., "Hierarchical Stochastic Frequency Constrained Micro-Market Model for Isolated Micro-grids", IEEE Transaction on Smart Grid, Vol. 15, No. 1, pp. 5-18, 2024, DOI:10.1109/TSG.2023.3266761.

[3] Zhang Z., Fang J., Dong C., Jin C., and Tang Y., "Enhanced Grid Frequency and DC-Link Voltage Regulation in Hybrid AC/DC Micro-grids Through Bidirectional Virtual Inertia Support", IEEE Transactions on Industrial Electronics, Vol. 70, No. 7, pp. 6931–6940, July 2023, DOI: 10.1109/TIE.2022.3203757.

[4] Tegling E., Andreasson M., Simpson-Porco J.W., Sandberg H., "Improving performance of droop-controlled micro-grids through distributed PI-control", In Proceedings of the American Control Conference (ACC), Boston, MA, USA, pp. 2321–2327, 6–8 July 2016, DOI:10.1109/ACC.2016.7525264.

[5] Schiffer J., Ortega R., Astolfi A., Raisch J., and Sezi T., "Conditions for Stability of Droop-Controlled Inverter-Based Microgrids", Elsevier, Automatica, Vol. 50, No. 10, pp. 2457–2469, 2014, DOI:10.1016/j.automatica.2014.08.009.

[6] Kölsch L., Wieninger K., Krebs S., and Hohmann S., "Distributed Frequency and Voltage Control for AC Micro-grids Based on Primal-Dual Gradient Dynamics", Elsevier , IFAC-PapersOnLine, Vol. 53, No. 2, pp. 12229-12236, 2020, DOI: 10.1016/j.ifacol.2020.12.1110.

[7] Dehkordi N.M., Sadati N., and Hamzeh M., "Fully Distributed Cooperative Secondary Frequency and Voltage Control of Islanded Microgrids", IEEE Transactions on Energy Conversion, Vol. 32, No. 2, pp. 675–685, June 2017, DOI: 10.1109/TEC.2016.2638858.

[8] Dhara P.K., and Rather Z.H., "Non-synchronous Inertia Estimation in a Renewable Energy Integrated Power System with Reduced Number of Monitoring Nodes", IEEE Transactions on Sustainable Energy, Vol. 14, No. 2, April 2023, DOI: 10.1109/TSTE.2022.3227603.

[9] Khayat Y., Naderi M., Shafiee Q., Batmani Y., Fathi M., Guerrero J.M., Bevrani H., "Decentralized Optimal Frequency Control in Autonomous Micro-grids", IEEE Transactions on Power Systems, Vol. 34, No. 3, pp. 2345–2353, 2019, DOI: 10.1109/TPWRS.2018.2889671.

[10] Eini M.K., Moghaddam M.M., Tavakoli A., and Alizadeh B., "Improving the stability of hybrid micro-grids by nonlinear centralized control in island performance", International Journal of Electrical Power and Energy Systems, Vol. 136, March 2022, 107688, DOI: 10.1016/j.egyr.2023.09.162.

[11] S. hrivastava, B. Subudhi, S. Das, "Distributed Voltage and Frequency Synchronisation Control Scheme for Islanded Inverterbased Microgrid", IET Smart Grid, vol. 1, No. 2, pp. 48–56, 2018, DOI:10.1049/iet-stg.2018.0020.

[12] Mohamad A.M.I., and Mohamed Y.A-R.I., "Investigation and Assessment of Stabilization Solutions for DC Micro-grid with Dynamic Loads", IEEE Transactions on Smart Grid, Vol. 10, No. 5, pp. 5735 – 5747, 2019, DOI: 10.1109/TSG.2019.2890817.

[13] Kerdphol T., Watanabe M., Mitani Y. and Phunpeng V., "Applying Virtual Inertia Control Topology to SMES System for Frequency Stability Improvement of Low-Inertia Micro-grids Driven by High Renewables", Energies, Vol. 12, No. 20, , 2019, DOI:10.3390/en12203902.

[14] Amin W.T. , Montoya O.D , V.M. Garrido, W. Gil-González and A. Garces, "Voltage and Frequency Regulation on Isolated AC Three-phase Micro-grids via s-DERs", IEEE Green Technologies Conference (GreenTech), Lafayette, LA, USA, 2019, DOI:10.1109/GreenTech.2019.8767133.

[15] Soni N., Doolla S., and Chandorkar M.C., "Analysis of frequency transients in isolated micro-grids", IEEE Transactions on Industry Applications, Vol. 53, No. 6, pp. 5940-5951, 2017,

DOI:10.1109/TIA.2017.2746619.

[16] Hassan M.A., "Dynamic Stability of an Autonomous Micro-grid Considering Active Load Impact with a New Dedicated Synchronization Scheme", IEEE Transactions on Power Systems, Vol. 33, No. 5, pp. 4994-5005, 2018, DOI:10.1109/TPWRS.2018.2798160.

[17] Ferraro P., Crisostomi E., Shorten R. and Milano F. , "Stochastic frequency control of grid-connected micro-grids", IEEE Transactions on Power Systems, Vol. 33, No. 5, pp. 5704-5713, 2018, DOI: 10.1109/TPWRS.2018.2821370

[18] Kundu S., Du W., Nandanoori S.P., Tuffner F., and schneider K., "Identifying Parameter Space for Robust Stability in Nonlinear Networks: A Micro-grid Application", American Control Conference (ACC), Philadelphia, PA, USA, 2019, DOI: 10.23919/ACC.2019.8814324.

[19] Krause P.C., Wasynczuk O., Sudhoff S.D., and Pekarek S., "Analysis of electric machinery and drive systems", New York: IEEE press, Vol. 2, 2002.

[20] Tang X., Deng W. and Qi Z., "Investigation of the Dynamic Stability of Micro-grid", IEEE Transactions on Power Systems, Vol. 29, No. 2, pp. 698 – 706, 2014, DOI: 10.1109/TPWRS.2013.2285585.

[21] Bottrell N., Prodanovic M., and Green T.C., "Dynamic stability of a micro-grid with an active load", IEEE Transactions on Power Electronics, Vol. 28, No. 11, pp. 5107-5119, 2013, DOI: 10.1109/TPEL.2013.2241455.

Authors Biographies

Zahra Mobini-Serajy received her M.Sc. degree in Electrical Engineering from Qazvin Azad University in 2012 and is currently a Ph.D. student at Azad University of Sari. Her research focuses on power electronics and micro-grids, with an emphasis on developing innovative solutions to improve energy systems. Zahra's academic journey has provided her with a strong foundation in the dynamics of power systems, and she is dedicated to contributing to advancements in modern electrical engineering.

Mehdi Radmehr received the B.Sc., M.Sc., and Ph.D. degrees in electrical Engineering from University of Tehran, Tarbiat Modares and Islamic Azad University (Science and Research Campus) all in Tehran, Iran, in 1996, 1998, 2006, respectively. He is a specializing in power electronics, motor drives and power. He has worked for mazandaran Wood and Paper Industries as an advisor since 1997 before starting his Ph.D. study. He has joined the scientific staff of Islamic Azad University, Sari Branch, Iran since 1998.

Alireza Ghorbani was born in Sari, Iran. He received the B.Sc. degree with honor from the University of Semnan, Iran, in 2009, the M.Sc. degree from Iran University of Science and Technology in 2011 and the Ph.D. degree with honor from the University of Shahed, Tehran, Iran, in 2016. He is currently an Assistant Professor with Islamic Azad University, Central Tehran, Iran. His current research interests include current mode integrated circuit design, low voltage, Low-Power and Energy-Efficient circuit and systems, and analog microelectronics and RF design.